



# EXPERIMENTAL INVESTIGATION OF A HUMIDIFICATION-DEHUMIDIFICATION DESALINATION UNIT WORKING UNDER BAGHDAD CONDITIONS

Zahra F. Hussain<sup>a,\*</sup>, Ahmed J. Hamed<sup>b</sup>, Abdul Hadi N. Khalifa<sup>b</sup>, Mohanad F. Hassan<sup>b</sup>, Fawaz A. Najim<sup>c†</sup>

<sup>a</sup> Air conditioning and Refrigeration Techniques Engineering Department Al-Mustaqbal University College, Babylon, 51001, Iraq

<sup>b</sup> Middle Technical University, Engineering Technical College, Baghdad, Iraq

<sup>c</sup> Former Ministry of Science and Technology-, Baghdad, Iraq

## ABSTRACT

At places far from the energy grid lines, freshwater is sometimes needed. Consequently, even countries with rich energy resources, such as the Arabian Gulf countries, have shown strong interest in desalination processes that often use renewable energy sources. In the present work, a desalination unit depending on the humidification-dehumidification principles is fabricated and tested under Baghdad, Iraq conditions. The HDH system under study consists of 6 parabolic trough solar collectors (PTSC) of a total aperture area of 8.772 m<sup>2</sup>, the humidifier, and the dehumidifier and a tracking system. The effects of salty water flow rate and the HDH air-water configuration cycles on the system performance are investigated. The results revealed that the maximum freshwater productivity is about 6.37 lit/day during the testing period (6 hours per day extended from 9 am to 15 hr); the average daily productivity is 1.062 lit/hr when the salty water flow rate is 1lit/min. Increasing salty water flow rate above 1 lit/min deteriorates the productivity of freshwater. The best configuration of the air-water cycle is the closed air open water circuit.

**Keywords:** Desalination; humidification- dehumidification; solar energy; parabolic trough collector

## 1. INTRODUCTION

Water is essential for life and is essential for sustainable growth as it is used in various areas of life such as; energy, agriculture, transport and industry. Humans and other forms of life rely on clean and fresh water. However, the most abundant water sources are the seas and oceans, but these waters need to be desalinated before use. Humidification - Dehumidification (HDH) is an important technique that has been extensively adapted to desalination. There are several studies on the process of HDH. These studies focus on evaluating performance and improving efficiency to improve solar desalination systems' freshwater production and reduce their costs.

The HDH solar desalination system's characteristics were studied by (Orfi, Laplante and Marmouch, 2004). Their study consists of two parts. Part one has presented the design and the construction of the HDH unit and studied the relationship between the evaporator and the condenser's temperatures. Part two presented the mechanism of heat and mass transfer in the unit parts. The mathematical results showed an optimum relationship between the mass ratio of water to air and freshwater production. (Al-Enezi, Ettouney and Fawzy, 2006) presented the HDH unit characteristics as a function of operating conditions; the study aimed to find the relation between the unit performance as a function of the mass ratio between the water and air streams (L/G), the water stream temperature and the cooling water temperature. It was found that the water production rate depended strongly on the hot water temperature, and water production was directly proportional to the air mass flow rate. (Yamali and Solmuş, 2007) studied a closed water open-air HDH unit's. A double passes flat plate solar heater was used to heat the inlet air to the desalination unit. An evacuated tube solar collector

was used to heat the inlet water. The effects of (L/G), the integrated the evacuated tube solar collector and the initial water temperature on the unit performance were introduced. The results showed that water productivity was decreased when the air heater is off the cycle.; the system's productivity was increased with the increase of the initial water temperature inside the storage tank. In Tunisia, on July day, a heat and mass transfer model for the HDH unit was presented by (Orfi, Galanis and Laplante, 2007). The theoretical model was used to optimize the HDH unit dimensions. The effect of (L/G) on the unit productivity and the inlet and outlet water temperature from the solar collector was studied. On the same path, the operating parameters for the HDH unit have been studied experimentally and theoretically by (El-Agouz, 2010); and addressed the effects of saline water level, water temperature and airflow rate on the humid air behaviour for a single HDH unit. Comparison between different HDH units has been presented by (Narayan *et al.*, 2010). For a clear view of the HDH systems' performance, thermal processes were represented on the psychrometric chart. The HDH unit components were reviewed and compared; the authors concluded that HDH is a promising technology. (Mayere, 2011) introduced a V-through solar collector of 8 m<sup>2</sup> to provide thermal energy to an HDH system's seawater. The system was analyzed experimentally and theoretically. In another work, an HDH system of 1000 lit/day productivity was designed and built by the Chinese Academy of Sciences and HIMIN Solar Co., Ltd and investigated experimentally by (Yuan *et al.*, 2011). The air was heated by a solar heater field, while solar collectors heated the water. Saline water was pre-treatment and post-treatment before entering the HDH unit. The combination between an HDH unit and a single-stage flash evaporation unit was investigated numerically by (Kabeel and El-Said, 2013). A two-dimensional heat and mass transfer analysis was introduced for the hybrid solar system using

\* Corresponding author. Email: [zahraa9.hussain9@gmail.com](mailto:zahraa9.hussain9@gmail.com)

the finite difference method; the productivity for different operating modes was compared. The results showed a general agreement between the HDH system's works with the single-stage flash evaporation unit. A mathematical model of the HDH unit under summer conditions was introduced by (He *et al.*, 2017); freshwater production, the flat plate solar collector's collection efficiency, and the gained output ratio were simulated and analyzed. (Shalaby, Bek and Kabeel, 2017) studied the performance of a solar-powered HDH unit. They assumed that the air temperature has little effect on water productivity; thus, they do not recommend using a solar air heater. On the other hand, water productivity was found directly proportional to the salty water temperature, so they are recommended to use a concentrating parabolic trough or evacuated tube collectors. Based on their recommendations, three points for future work were suggested. (Moumouh, Tahiri and Balli, 2018), so they investigated a prototype HDH unit, and analyzed the heat and mass transfer for water and air that affected the unit performance. The results showed that productivity was affected positively by increasing the brackish water mass flow rate. The exit water temperature from the dehumidification unit had a direct proportion with inlet water temperature and an inverse proportion with the inlet mass flow rate of water. Mahmoud *et al.*, 2018 (Mahmoud, Fath and Ahmed, 2018) introduced a new design for a solar disinflation unit. The unit was powered by different energy sources such as direct solar energy and the energy from a PV unit. The effects of the basin water height, L/G and solar concentrating ratios on the unit performance were investigated. The experimental work was followed by a transient mathematical model based on the conservation of mass and energy to predict the HDH unit performance. The results showed that the basin water height and the mass flow rate affected negatively on water production. Integrated PV panels with solar concentrators lead to an increase the freshwater productivity. The integrated of solar heater and wind tower with a HDH unit was studied numerically by (Sachdev, Gaba and Tiwari, 2020); both closed and open air water cycle were analyzed. A mathematical based on energy and mass balance as well as heat and fluid flow model for each unite components were introduced. The effect of condensing temperature and salty water flow rate on the HDH unit's performance integrated with a heat pump was studied theoretically by (Pourafshar, Jafarinaemi and Mortezaipour, 2020); a photovoltaic- thermal unit heated the salty water, a heat pump unit controlled the condensing temperature. The performance of a simple passive solar still was introduced by (Manjunath *et al.*, 2020). An evaporative cooler used wet cloth cotton to cool the water, and then the cold water was sprayed on the still glass cover.

In this work, the performance of a humidification –dehumidification desalination (HDH) is studied experimentally. The HDH unit consists of six series connecting parabolic trough solar collectors of 8.772 m<sup>2</sup> total aperture area. A humidifier, dehumidifier, fan, pumps and other accessories that consist of the HDH unit is built in Baghdad, Iraq latitude 33.33° N and longitude 44.14 °E. The experimental work was achieved in August 2020. The effects of salty water flow rate and air circuit configuration on the unit performance are studied.

## 2. METHODS AND MATERIALS

Heat losses for PTSC result from the convection and radiation from the receiver tube to the ambient affect the PTSC thermal performance. Thus, to calculate the collector's heat loss rate, the overall heat transfer coefficient UL should be addressed first as follows (Li and Wang, 2006).

$$U_L = \left[ \frac{A_{abs}}{A_g} (h_{c,g-amb} + h_{r,g-amb}) + 1/h_{r,abs-g} + \ln(D_{g,in}/D_{abs,o}) / 2\pi k_{eff} \right]^{-1} \quad (1)$$

Where  $A_{abs}$  is the area of the absorber (m<sup>2</sup>),  $A_g$  is the area of glass cover (m<sup>2</sup>),  $D_{g,in}$  is the inside diameter of the glass cover (m),  $D_{abs,o}$  is the outside diameter of the absorber (m) and  $k_{eff}$  is the thermal conductivity that the stationary air should have to transfer the same

amount of heat as moving air. A suggested correlation to calculate for ( $k_{eff}$ ) (W/m.K) is (Kreith, Manglik and Bohn, 2012)

$$\frac{k_{eff}}{k_{air}} = 0.386 \left[ \frac{\ln \left( \frac{D_{g,in}}{D_{abs,o}} \right)}{b^{3/4} \left( D_{abs,o}^{-3/5} + D_{g,in}^{-3/5} \right)^{5/4}} \right] \left[ \frac{Pr_{air}}{0.861 + Pr_{air}} \right]^{1/4} (Ra_b)^{1/4} \quad (2)$$

where Rayleigh number  $Ra_b$  is based on the temperature difference across the gap.  $Pr_{air}$  is the Prandtl number of air in the annulus ( $k_{air}$ ) is the thermal conductivity of air (W/m.K) and (b) is evaluated as:

$$b = 0.5(D_{g,in} - D_{abs,o}) \quad (3)$$

The Rayleigh Number of air ( $Ra_b$ ) is:

$$Ra_b = (g\beta_{air}(T_{abs} - T_g)b^3)/(\alpha_{air}\nu_{air}) \quad (4)$$

where (g) as the gravitational acceleration (m/s<sup>2</sup>), ( $\beta_{air}$ ) is the volumetric thermal expansion coefficient of air (K<sup>-1</sup>), ( $\alpha_{air}$ ) is the thermal diffusivity of air (m<sup>2</sup>/s) and ( $\nu_{air}$ ) is the kinematic viscosity of air (m<sup>2</sup>/s).

The convection heat transfer coefficient ( $h_{c,g-amb}$ ) between glass and ambient and can be calculated as follows (Jacobson *et al.*, 2006; Kreith, Manglik and Bohn, 2012)

$$h_{c,g-amb} = Nu_a k_a / D_g \quad (5)$$

Two equations defined the Nusselt number of air ( $Nu_a$ ) (Jacobson *et al.*, 2006):

$$Nu_a = 0.4 \times 0.54 \cdot Re_a^{0.53} \quad \text{for } 0.1 < Re_a < 1000 \quad (6)$$

$$Nu_a = 0.3 \cdot Re_a^{0.6} \quad \text{for } 1000 < Re_a < 50000 \quad (7)$$

Reynolds number ( $Re_a$ ) of air is calculated by the following equation (Kreith, Manglik and Bohn, 2012):

$$Re_a = (\rho_a V_a D_g) / \mu_a \quad (8)$$

where  $k_a$ ,  $\rho_a$ ,  $V_a$  and  $\mu_a$  are thermal conductivity, density, velocity and viscosity of air, respectively,  $D_g$  Glass cover diameter (m).

The radiation heat transfer coefficient between the glass and the ambient can be calculated as follows (Li and Wang, 2006):

$$h_{r,g-amb} = \epsilon \sigma (T_g + T_{amb})(T_g^2 + T_{amb}^2) \quad (9)$$

The radiation heat transfer coefficient between the receiver tube and the glass tube is as follows:

$$h_{r,abs-g} = \sigma (T_{abs} + T_g)(T_{abs}^2 + T_g^2) / \left( \frac{1}{\epsilon_{abs}} + \frac{1 - \epsilon_g}{\epsilon_g} \left( \frac{A_{abs}}{A_g} \right) \right) \quad (10)$$

where  $T_{abs}$  is the absorber temperature (K),  $T_g$  : is the glass cover temperature (K),  $\epsilon_{abs}$  and  $\epsilon_g$  are the emittance of absorber and glass cover, respectively, and  $\sigma$  is the Stefan Boltzmann constant.

The heat transfer from the receiver tube to the water can be characterized either by turbulent or laminar flow conditions according to Reynolds number ( $Re_f$ ) of the fluid (Garg, 2000)

$$Re_f = 4m / (\pi D_{abs} \mu_f \rho_{collectors}) \quad (11)$$

$Nu_f$  is the Nusselt number of the fluid, for laminar flow is given by Eq. (12) and for turbulent flow by Eq. (13).

$$Nu_f = 3.7 \quad \text{Ref} < 2200 \quad (12)$$

$$Nu_f = (f_f/8) Re_f Pr_o / \left( 1.07 + 12.7 \sqrt{(f_f/8)} \left[ \frac{Pr_o}{f_f} - 1 \right] \right) \quad \text{Ref} > 2200 \quad (13)$$

Where  $f_f$  is the friction factor of the tube; the friction factor for smooth pipes is given by:

$$f_f = [0.79 \ln(Re_f - 1.6)]^{-2} \quad (14)$$

The fluid heat transfer coefficient,  $h_f$  is evaluated as follows (Thepa *et al.*, 1999)

$$h_f = (Nu_f k_f) / D_{asb,i} \quad (15)$$

Where  $m$ ,  $\mu_f$ ,  $k_f$ , and  $Pr_f$  are the mass flow rate, viscosity, thermal conductivity and Prandtl number of the water, respectively, and  $D_{asb,i}$  is the inner receiver diameter (m).

The rate of heat transfer to the water in the tube depends on the overall heat transfer coefficient between the outer and inner surfaces of the copper tube ( $U_o$ ). The overall heat transfer coefficient can be calculated as follows (Li and Wang, 2006):

$$U_o = \left[ \frac{1}{U_L} + \frac{D_{asb,o}}{h_f D_{asb,i}} + Rf_c + \frac{D_{asb,o}}{2k_{abs}} \ln \frac{D_{asb,i}}{D_{asb,o}} \right]^{-1} \quad (16)$$

Where  $k_{abs}$  is the thermal conductivity of the copper tube (W/m.K), and  $Rf_c$  is the fouling factor.

The collector efficiency factor ( $F'$ ) is calculated as follows:

$$F' = U_o / U_L \quad (17)$$

Equation (17) can be re-written as follows (Duffie and Beckman, 2013)

$$F' = \frac{1/U_L}{[1/U_L + D_{asb,o}/h_f D_{asb,i} + \{(D_{asb,o}/2k_{abs}) \ln(D_{asb,i}/D_{asb,o})\}} \quad (18)$$

Where  $D_{asb,i}$  is the inside diameter of the copper tube (m), ( $h_f$ ) is the heat transfer coefficient inside the tube (W/m<sup>2</sup>.°C), and  $U_o$  is the overall heat transfer coefficient (W/m<sup>2</sup>.K). The heat removal factor  $F_R$  is given as follows:

$$F_R = (\dot{m} C_{pf} / A_{abs} U_L) [1 - \exp(-A_{abs} U_L F' / \dot{m} C_{pf})] \quad (19)$$

Where  $C_{pf}$  is the specific heat of the water (kJ/kg.K).

The collector flow factor  $F''$  is:

$$F'' = F_R / F' \quad (20)$$

Substitute Eq. (19) into Eq. (20) yield:

$$F'' = (\dot{m} C_{pf} / A_{abs} U_L F') [1 - \exp(-A_{abs} U_L F' / \dot{m} C_{pf})] \quad (21)$$

The useful heat gain  $Q_u$  by the water can be found as follows (Duffie and Beckman, 2013)

$$Q_u = \eta_{th} A_a I_b - U_L (T_{abs} - T_{amb}) A_{abs} \quad (22)$$

Where,  $A_a$  is the collector aperture area (m<sup>2</sup>), and  $I_b$  is the beam of solar radiation (W/m<sup>2</sup>).

It is more reasonable to define the useful heat gain in terms of inlet water temperature and the heat removal factor (Kalogirou *et al.*, 2016).

$$Q_u = A_a F_R [S - U_L (T_f - T_{amb}) / C] \quad (23)$$

Where  $C$  is the concentration ratio of the PTSC

The heat gained by the receiver is transferred to the water, as in the following equation (Garg and Prakash, 1997).

$$Q_u = m \cdot c_p (T_{f,o} - T_{f,i}) \quad (24)$$

Where:  $T_{f,i}$ ,  $T_{f,o}$  and  $T_{amb}$  are the inlet water, outlet water and ambient temperatures, respectively.

The ratio of the useful energy to the total solar radiation incident on the collector is called the collector thermal efficiency ( $\eta_{th}$ ), and can be written as

$$\eta_{th} = Q_u / A_a I_b \quad (25)$$

Depending on equations (23) and (25) another form of thermal efficiency can be written as: (Mazloumi, Naghashzadegan and Javaherdeh, 2008):

$$\eta_{th} = F_R [\eta_o - U_L (T_f - T_{amb}) / I_b C] \quad (26)$$

The collector thermal efficiency depending on the water's heat through the copper tube is as follows (Mazloumi, Naghashzadegan and Javaherdeh, 2008).

$$\eta_{th} = m C_p (T_{f,o} - T_{f,i}) / I_b A_a \quad (27)$$

The mathematical model of the humidifier that shown in Figure 1 is given by the following equations:

The mass balance equation is:

$$L - L - dL + G - G - G \cdot d\omega = 0 \quad (28)$$

$$dL = G \cdot d\omega \quad (29)$$

Where,  $L$  is the mass flow rate of water through humidifier (kg/s),  $dL$  is the increment in the mass flow rate of water (kg/s),  $G$  is the mass flow rate of air through the humidifier (kg/s), and  $d\omega$  is the increment in the moisture content of air (kgw/kg)

According to Figure (1), the energy balance of an element through the humidifier is (Ettouney, 2005)

$$(L + dL) \cdot (h_w + d h_w) + G \cdot h_a = L \cdot h_w + (G + G \cdot d\omega) \cdot (h_a + d h_a) \quad (30)$$

After re-arranging Eq. (30) and substitute the enthalpy of water by ( $C_{pw} \cdot T_w$ ) yields:

$$G \cdot d h_a = L \cdot C_{pw} \cdot T_w + C_{pw} \cdot T_w \cdot dL \quad (30a)$$

Substitute Eq. (29) into Eq. (30a) yields::

$$dT_w = \frac{G}{L} \cdot (d h_a / C_{pw} - T_w \cdot d\omega) \quad (30b)$$

The change of the enthalpy in a wet humidifier is the summation of sensible and latent heat change of water (Stoecker and Jones, 1982):

$$dq_t = dq_{lat} + dq_{sen} \quad (31)$$

The latent heat can be written as:

$$dq_{lat} = h_{diff} \cdot (\omega_s - \omega) \cdot h_g \cdot dA \quad (32)$$

While the temperature difference between the water and air causes a sensible heat transfer from the water to the air:

$$dq_{sen.} = h_c \cdot (T_w - T_a) \cdot dA \quad (33)$$

Where,  $h_{diff.}$  is the mass transfer coefficient (kg/m2s), and  $h_c$  is the heat transfer coefficient (W/m2.K)

The enthalpy of moist air can be written as (Stoecker and Jones, 1982):

$$h_{air} = (C_{pa} + C_{pv}\omega)T_a + h_{fg}\omega \quad (34)$$

If the air is saturated at bulk water temperature, then the enthalpy of saturated is:

$$h_{a,sat} = c_{pa} \cdot T_w + \omega_{sat} \cdot (h_{fg} - c_{pv} \cdot T_w) \quad (35)$$

Subtract Eq. (37) from Eq. (38) yields:

$$(h_{a,sat} - h_a) = (c_{pa} + \omega_{sat} \cdot c_{pv}) \cdot T_w - (c_{pa} + \omega \cdot c_{pv}) \cdot T_a + (\omega_{sat} - \omega) \cdot h_{fg} \quad (36)$$

Many assumptions are used to simplify Eq. (36) (Stoecker and Jones, 1982). The first assumption is that the difference in moisture content between the saturated and moist air is very small then the  $(c_{pa} + \omega_{sat} \cdot c_{pv})$  of the right hand of Eq. (37) can be assigned as the specific heat of the air-water vapour mixtures ( $c_{pm}$ ). This term can be calculated as follows:

$$c_{pm} = (c_{pa} + \omega \cdot c_{pv}) = (c_{pa} + \omega_{sat} \cdot c_{pv}) \quad (37)$$

where,  $c_{pa}$  and  $c_{pv}$  are the specifics heats of air and water vapour (kJ/kg. K).

The second assumption that the enthalpy of liquid water is too small as compared with that of the dry saturated vapour, and then the enthalpy of evaporation of water  $h_{fg}$  can be assumed equal to the enthalpy of dry saturated air.

By using the two assumptions above and re-arranging Eq. (36) yields:

$$T_w - T_a = [(h_{a,sat} - h_a) - (\omega_{sat} - \omega) \cdot h_g] / c_{pm} \quad (38)$$

After substituting Eqs. (32), (33) and (38) into Eq. (31) yields:

$$dq_t = h_{diff.} [h_c / c_{pm} \cdot h_{diff.} \cdot (h_{a,sat} - h_a) + (1 - h_c / c_{pm} \cdot h_{diff.}) \cdot (\omega_{sat} - \omega) \cdot h_g] \cdot dA \quad (39)$$

The Merkel theory [28] states that water's mass flow rate through humidifier is constant. Thus, the variation of mass flow rate due to evaporation of water is neglected, and then the second terms between brackets in the right hand of Eq. (39) can be neglected:

$$dq_t = (h_c \cdot dA / c_{pm}) \cdot (h_{a,sat} - h_a) \quad (40)$$

The amount of total heat transferred through the humidifier is as follows::

$$dq_t = m_w C_{pw} \cdot dT_w \quad (41)$$

Equating (40) and (41) yields:

$$m_w C_{pw} \cdot dT_w = (h_c \cdot dA / c_{pm}) \cdot (h_{a,sat} - h_a) \quad (42)$$

The term  $(h_{a,sat} - h_a)$  in Eq. (42) is the increment of element enthalpy difference.

The humidifier effectiveness is the ratio of the actual to the maximum energy transfer through the humidifier and can be written as:

$$\epsilon = (h_{a,e} - h_{a,i}) / (h_{a,sat} - h_{a,i}) \quad (43)$$

The enthalpy balance analogy equation is:

$$\dot{m}_{air} \cdot (h_{air,out} - h_{air,in}) = h_{diff.} \cdot a \cdot V \left[ \frac{(h_{w-in} - h_{air,out}) - (h_{w-out} - h_{air,in})}{\ln\{(h_{w-in} - h_{air,out}) / (h_{w-out} - h_{air,in})\}} \right] \quad (44)$$

The volumetric mass transfer coefficient ( $h_{diff.} \cdot a \cdot V$ ) in Eq. (44) is used to size and select the humidifier's material properties. The equation of volumetric mass transfer coefficient for forced draft humidifier and ( $L/G$ ) of  $0.1 < \frac{L}{G} < 2$  is (Nawayseh *et al.*, 1999):

$$h_{diff.} \cdot aV / L = 0.53 - 0.22 \cdot \log(L/G) \quad (45)$$

Where  $a$  is the surface area of the packing per unit volume ( $m^{-1}$ ) and  $V$  is the volume of the packing ( $m^3$ ).

Refers to Figure 2, the dehumidifier energy balance is between the saturated air streams and the coolant water flowing through the tubes and can be written as (Ettouney, 2005)

$$\dot{m}_{cw} C_{pcw} (T_{cwo} - T_{cwi}) = \dot{m}_a (h_o - h_i) \quad (46)$$

The heat gain by the outer surface of the heat exchanger is:

$$\dot{m}_{cw} C_{pcw} (T_{cwo} - T_{cwi}) = U_c A_c LMTD_c \quad (47)$$

where,  $\dot{m}_{cw}$  is the mass flow rate of coolant water (kg/sec),  $\dot{m}_a$  is the mass flow rate of air (kg/sec),  $T_{cwi}$  and  $T_{cwo}$  are the inlet and outlet coolant water temperature ( $^{\circ}C$ ),  $h_o$  and  $h_i$  are the enthalpies of inlet and outlet air (kJ/kg), and  $LMTD_c$  is the logarithmic mean temperature difference between coolant water and air:

$$LMTD_c = (T_{cwi} - T_{cwo}) / \ln\{(T_{ac} - T_{cwo}) / (T_{ac} - T_{cwi})\} \quad (48)$$

where,  $T_{ac}$  is the saturated air temperature (K).

The overall transfer coefficient of the dehumidifier  $U_c$  can be written as:

$$\frac{1}{U_c} = \frac{1}{h_{ci}} * \frac{r_{co}}{r_{ci}} + Rf_c + r_{co} \cdot \{\ln(r_{co}/r_{ci}) / k_c\} + 1/h_{co} \quad (49)$$

where,  $Rf_c$  is the fouling factor, ( $r_{ci}$ ) and ( $r_{co}$ ) are the inner and outer radius of the heat exchanger tubes (m) respectively, ( $h_{ci}$ ) and ( $h_{co}$ ) are the inner and outer heat transfer coefficient of the dehumidifier tube. (W/m2.K), and  $k_c$  is the thermal conductivity of the copper tube (W/m.K).

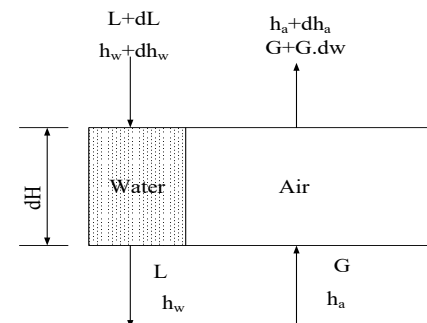
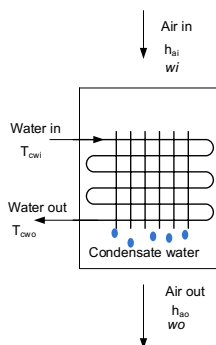


Fig. 1 The heat and mass balance of the humidifier



**Fig. 2** Schematic diagram of the heat and mass analysis of the dehumidifier

### 3. EXPERIMENTAL WORK

A water solar desalination system based on solar-powered HDH units is fabricated and instrumented to examine various operating parameters' effect on the unit performance. The unit is tested under weather conditions of Baghdad, 33.33°N latitude, 44.14°E longitude.

The solar-powered HDH unit consists of six parabolic trough solar collectors, a humidifier, a dehumidifier, a centrifugal fan, and a rotary pump. Figure 3 shows the schematic diagram of the unit.

The dimension of a single PTSC is 0.86 m aperture width and 1.7 m long of 1.462 m<sup>2</sup> aperture area. The total aperture area of the collectors is 8.772 m<sup>2</sup>. The PSTC reflector is made of stainless steel. The receiver is a copper tube of 15 mm outer diameter painted by a matt black colour and contained in a glass tube of 25 mm inner diameter and 30 mm outer diameter. Figure 4 shows the shape of the PTSC. A single-axis solar tracking system is used to direct the PTSCs towards the sun throughout the day time. The solar tracking system consists of an AC motor of 250 W and 1360 rpm. A gearbox of a reduction ratio of (40-1) rpm is installed at the AC motor shaft. A sprocket gear of a diameter of 0.08 m is installed on the gearbox shaft; another sprocket gear of a diameter of 0.16 m is installed on the 3rd collector centre. A metal chain connects the two sprocket gears. The motor is turned on by a signal received from photocells installed on the 3rd collector. Connecting road is used to transfer the movement from the 3rd collector to the rest collectors, as shown in Figure 5.

The evaporation of the hot salty water is achieved at the humidifier. The direct contact between the sprayed salty hot water and the ambient air tends to evaporate the water. Thus, the humidifier consists of: an aluminium case with a thickness of 0.007 m, the overall height of the humidifier case is 2 m, and the net height is 1.3 m. The cross-sectional area of the humidifier case is 0.3 × 0.3 m, as shown in Figure 6. A PV packing of 0.7 m height with a cross-sectional area of 0.3 × 0.3 m is inserted in the humidifier. The salty water is sprayed at the humidifier top at an elevation of 0.25 m above the packing using a shower. The moist air enters the humidifier from the bottom through a convergent duct, while the saturated air leaves the humidifier from the top. The salty water is collected at the humidifier bottom; a 0.013 m pipe diameter is brazed at the tank base to drain the salty water.

The objective of the dehumidifier is to extract the water vapour from the saturated air leaving the humidifier. The dehumidifier consists of an aluminium case of thickness 0.007 m, 0.4 m length and a cross-sectional area of 0.4 × 0.2 m. The condensate is collected and drained from the dehumidifier case bottom. Four condensers of 8 rows and 2 columns each are enclosed in the dehumidifier case. Each condenser of the four condensers is fed by water separately. The condensers tube is made from copper of a 9 mm inner diameter. Aluminium fins of thickness 0.002 m are distributed along the pipe uniformly in the manner of 5 fins per 1 cm of pipe length. Figure 7 shows the photograph of the dehumidifier.

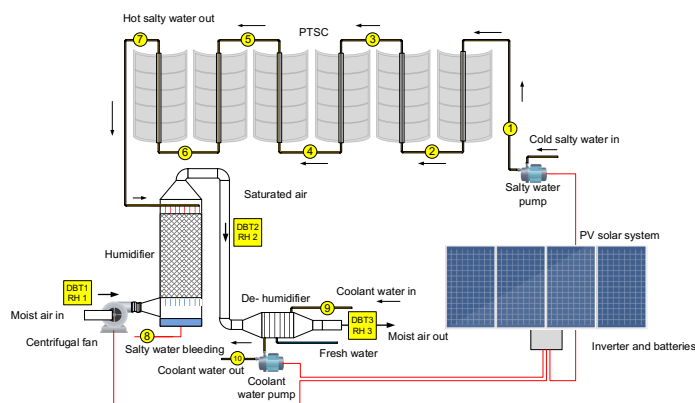


**Fig. 3** Schematic diagram of the HDH unit

Two water pumps are used to supply the system with water. The first pump is used to supply the dehumidifier with coolant water, while the second is used to pump the salty water through the PTSC and then to the humidifier. The maximum pump flow rate is 65 lit/min, 250 W capacity and the maximum head is 6 m. A centrifugal fan is used to circulate the air through the humidifier and dehumidifier. The volume flow rate pumped by the fan is in the range of 2400 to 6000 m<sup>3</sup>/hr. The fan power is 220 W, and the voltage drop is 220 V. PV solar system is used to power the pumps, fan, tracking system and the Arduino. The PV system is an OFF grid solar PV system consisting of four solar PV panels, each 2 m long and 1 m in width. The capacity of each PV panel is 360 W. The short circuit current is 9.12 A. The open circuit's voltage is 39.5 V. The four PV panels are used to generate a maximum power of 1440 W. A pure sine wave inverter of the maximum power point tracker is 1500W, and input DC volt is 145VDC is used to convert the DC to AC current. During the day time, the solar PV system powered the HDH components directly from the converted solar radiation, and no batteries need. Since the power supply in Iraq is not stable, two batteries connected in series are used to store the power generated, and this power is used when the grid supply is shutdown. Each battery can supply a DC current of 200 Ah, and the voltage drop of the battery is 12V. Figure 8 shows the HDH unit configuration. Table 1 shows the specifications of the PTSC.

Different types of measurements devices are used to measure the variation of key variables along 24 hrs, as follows: Water temperature is measured at 10 points, as shown in Figure 3. Type DS18B20 sensor is used for the water temperature measurement, the sensor temperature range of -55 to 125°C., according to the sensor manufacturer, the accuracy of those sensors over the temperature range from -10 to 85°C is ±0.5°C. Seven sensors of the type DS18B20 are used to measure the water temperature at the inlet and outlet at each PTSC. Two sensors are used to measure the inlet and outlet coolant temperatures at the condenser. Besides, one sensor is used to measure the outlet temperature from the humidifier. All measured data for 24 hr. are stored in a micro card adapter reader of types SDHC. Two properties of air, namely the dry bulb temperature (DBT) and the relative humidity (RH), are measured using a type DHT22 sensor. The primary sensor consists of two sensors; the first one is a thermistor to measure air temperatures in the range -40 to 80°C, with an accuracy of ±0.5°C as per the manufacturer data. The second is a capacitive humidity sensor, reading range is 0 to 100% RH, with an accuracy of ±2 % RH according to the manufacturer data. Three sensors are used to measure the air DBT and RH at the inlet and the humidifier's outlet.

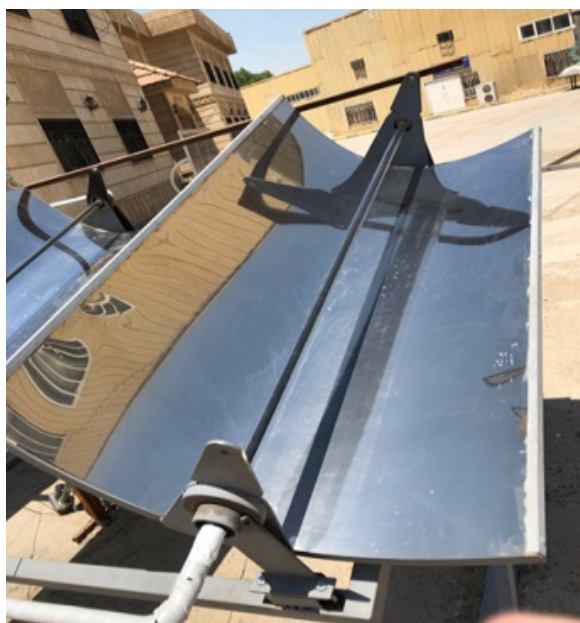


**Fig. 4** The PTSC



**Fig. 7** The dehumidifier



**Fig. 8a** front view of the HDH unit

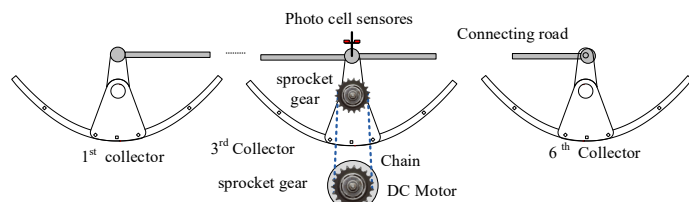


**Fig. 5** The solar tracking system details

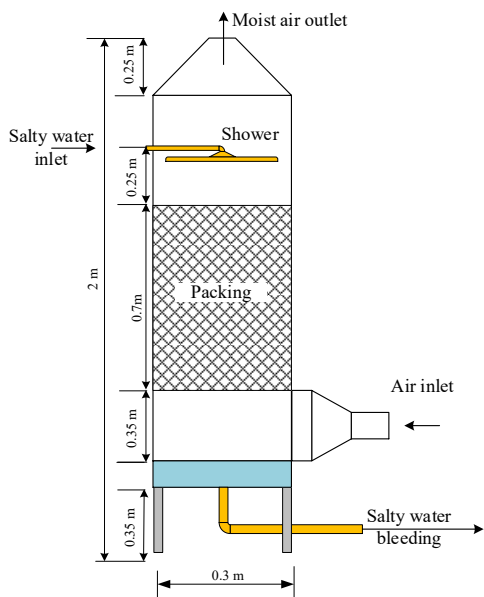


**Fig. 6** Schematic diagram of the humidifier



**Fig. 8b** Back view of the HDH unit

The water productivity is calculated by multiplying the water level in a known cross-sectional tank. The water level is measured using a water level sensor of type REES52. The operating distance range is 2 to 400 cm. the accuracy given by the manufacturer is 3 mm. The water volume flow rate is measured using a type YF-S201 sensor. The range of the measured flow meter is from 1 to 30 l/min. Three sensors are used to measure the salty water's volume flow rate; the other one is used to measure the coolant water flow rate to the dehumidifier. Air volume flow rate through the humidifier is calculated by measuring the airspeed through a given cross-sectional area duct; then, it is multiplied by the duct's cross-sectional area. The digital manometer model DA40 measures the speed of the air. There are two probes equipped with a manometer. The first one is the AP275 probe with a measuring range of 0.2 to 40 m/s. The second probe is AP100 with a measuring range of 0.3

to 35 m/s. The reading resolution is 0.01 m/s, the accuracy of the manometer given by the manufacture is  $\pm 1.0\%$  of reading  $\pm 1$  digit. Arduino is used to collecting the data from instrumentations and stored it in an SD card. The Arduino is also used to control the movement of the tracking motor system. Table 2 shows the uncertainty of the measurements devices.

**Table 1** The specifications of the PTSC

Variable	measured	unit
collector reflector length (m)	1.7	m
Collector aperture width	0.86	m
Collector aperture area	1.462	m <sup>2</sup>
Number of collectors	6	
Total aperture area	8.772	m <sup>2</sup>
Inside diameter of the absorber tube	0.012	m
Outside diameter of the absorber tube (for PTC)	0.015	m
Inside diameter of the glass tube cover (m)	0.025	m
Outside diameter of the glass tube cover (m)	0.03	m
Mass flow rate of salty water	0.8 to 1.2	Lit/min.
L/G	1.2	--
Mass flow rate of coolant water	2	Lit/min.

**Table 2** Absolute Accuracy

Variables	Accuracy error
DS18B20 Collector water temperature	$\pm 0.27^\circ\text{C}$
DHT22 Humidifier air relative humidity	$\pm 0.03\%$
DHT22 Air temperature	$\pm 0.91^\circ\text{C}$
DHT22 Dehumidifier air relative humidity	$\pm 0.1\%$
DHT22 Dehumidifier air temperature	$\pm 0.61^\circ\text{C}$
YF-S201 Collector water volume flow rate	$\pm 0.015\% \text{ m}^3/\text{hr}$
YF-S201 Dehumidifier water volume flow rate	$\pm 0.01\% \text{ m}^3/\text{hr}$
REES52 Water level	$\pm 0.01\% \text{ mm}$

#### 4. RESULTS AND DISCUSSIONS

The experimental work was performed in Baghdad in August 2020. The study parameters are the volume flow rate of salty water through the PTSC and the air cycle configuration. Five salty water flow rates are studied; namely, 0.6, 0.8, 0.9, 1 and 1.2 lit/min, and two air-water configuration circuits are investigated. These are the open-air- open water (OAOW) cycle and closed air – open water cycle (CAOW). It is planned to study the HDH performance under the closed air - closed water (CACW) cycle. Still, it is found that in summer, the outlet water temperature from the humidifier is less than that of the entering water temperature to the PTSC. Thus, the performance of the HDH unit under (CACW) configuration is ignored.

Figure 9 shows the main three parameters that affected the HDH unit performance: the solar radiation, ambient temperature, and relative humidity for Baghdad city. Meteonorm 7.3 package is used to obtain the weather data for Baghdad. The solar radiation is the average of the period extended from 1991 to 2010. In contrast, the ambient temperature and the relative humidity are the period's averages extended from 2000 to 2009.

The effect of the volume flow rate of salty water on the water outlet temperature from the PTSC is shown in Figure 10. It can be observed from the figure that, as the volume flow rate of the water through the PTSC system decreases, the leaving temperature increases accordingly. The maximum outlet temperature is for the volume flow rate of 0.8 lit/min, and the minimum is 1.2 lit/min. The outlet temperature from the PTSC is not the primary variable of the problem under study. The main parameter in this work is the rate of freshwater productivity.

The text of the paper (except the abstract) must be formatted in two-column. If any of the figures or tables is too wide to be placed in one column, they may be placed at the top or bottom of a page as one-column. Manuscripts must be written in clear, concise and grammatically correct English (either American or British style but not a mixture of both). Papers that do not conform to these requirements will be returned to the authors without review.

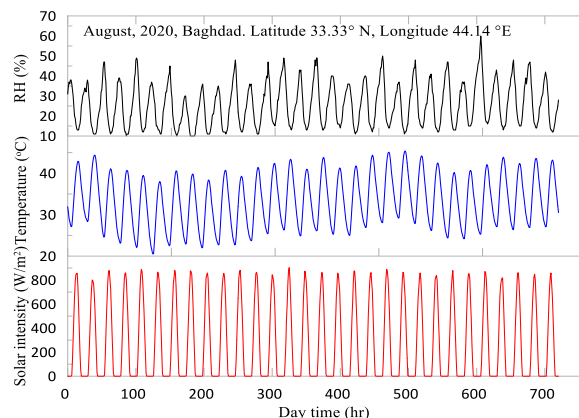


**Fig. 9** Weather data for August 2020 at Baghdad, Iraq

The effect of salty water flow rate on freshwater productivity is shown in Figure 11; it can be seen in the figure that as the salty volume flow rate of water increases, the freshwater productivity increases. Freshwater productivity decreases for the salty water flow rate of more than 1 lit/min due to the reduction in dry bulb temperature (DBT) of the air entering the humidifier, as shown in Figure 12. The coolant water reduction tends to reduce the temperature difference between coolant water and DBT of saturated air in the dehumidifier; thus, less water vapour condenses. While for low salty water flow rate, most coolant water is used to extract the sensible heat rather than condensing the airborne water vapour. The best equilibrium point between sensible and latent heat is at a 1 lit/min flow rate.

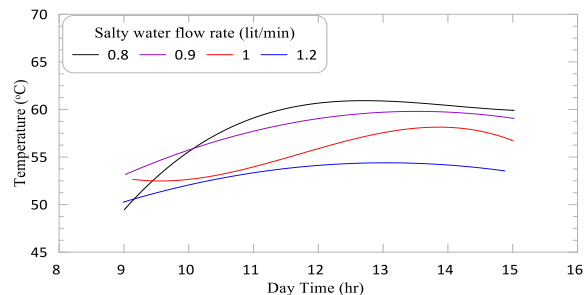


**Fig. 10** The effect of the volume flow rate of salty water on the leaving water temperature from PTSC

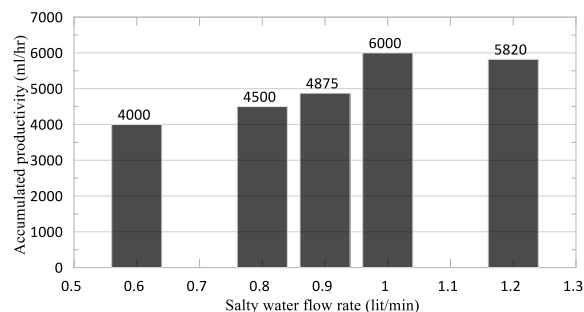
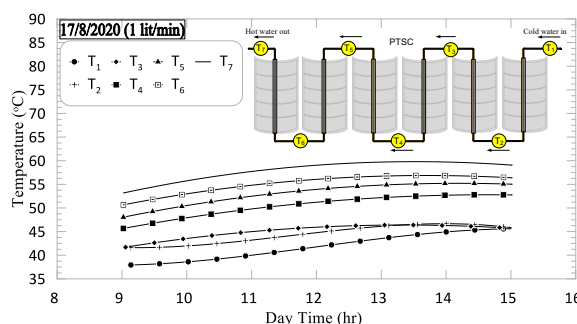


**Fig. 11** The effect of the saltwater flow rate on freshwater productivity

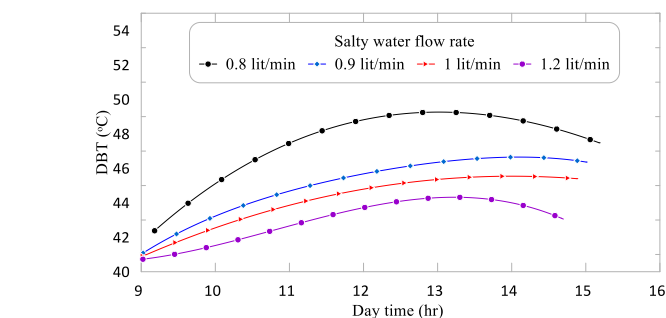
The variation of accumulated freshwater productivity with time for the different salty water flow rate is shown in Figure 13. A similar trend of accumulated water productivity can be observed for all the salty water

flow rates. It can be seen in this figure, the accumulated water productivity at a salty-water flow rate of 1.2 lit/min is higher than that for 1lit/min till time 13 hr. After that, the 1 lit/min produced more water compared with other salty water flow rates. There is no clear explanation for this phenomenon, although the test has been repeated several times at flow rates of 1 and 1.2 lit/min. It is believed that the humidifier's performance may be improved after hour 12.00 hr is due to the decrease in the relative humidity of the outside air, which allows it to carry more water vapour after this period, as illustrated in Figure 14. It can be concluded that the optimum salty water flow rate that can produce the relatively highest freshwater is 1 lit/min. Thus, the rest tests are performed at 1 lit/min.

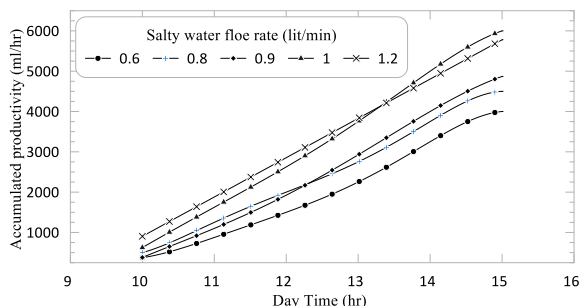
Figure 15 shows the performance of PTSC when the salty water flow rate is 1 lit/min. The figure shows that the outlet salty water temperature from each PTSC unit increases due to continuous heating of water from the 1st to the 6th collector.



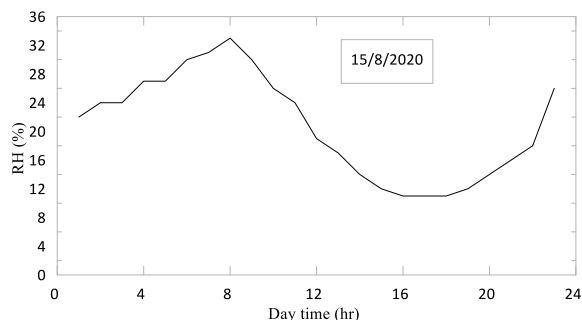
**Fig. 15** Salty water outlet temperature from each collector



**Fig. 12** The effect of salty water flow rate on the exit DBT from the humidifier



**Fig. 13** The effect of salty-water flow rate on the accumulated freshwater productivity



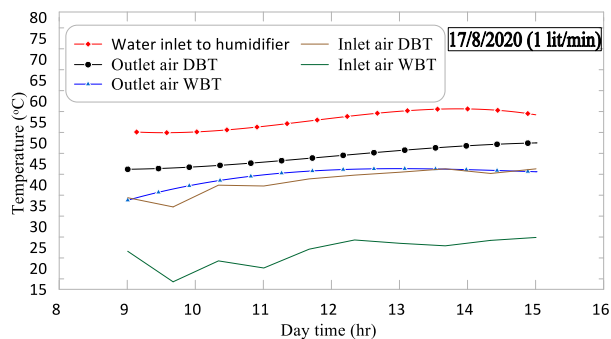
**Fig. 14** Outdoor relative humidity on 15 August 2020

Figure 16 shows the effect of the entering salty water temperature on the humidifier's outlet air conditions. The observation that the significant difference between the inlet air DBT and WBT is reduced when the air humidified in the humidifier. This means significant moisture is added to the outlet air. This figure also shows that the closeness between the DBT and WBT of the leaving air is at noon period, which means that the humidifier's higher performance can be achieved at this time.

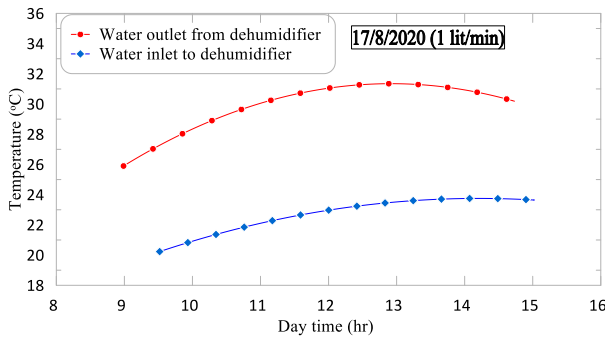
The thermal load imposed on the dehumidifier can be described by the difference between the coolant water's inlet and outlet temperature, as shown in Figure 17. It can be noticed that the maximum difference between the inlet and outlet temperature is at noon, which means that the maximum quantity of freshwater can be produced at that time.

The comparison between the freshwater productivity of open and closed air cycle for a salty water flow rate of 1 lit/min is shown in Figures 18 and 19. The figures show that the closed air cycle gave higher hourly and daily productivity of 1.062 lit/hr and 6.37 lit/day, respectively, during the testing period of 6 hours per day compared with that for the open-air cycle. The increase in water productivity for the closed air cycle is due to the reduction in DBT of the air entering the humidifier compared with that for the open-air cycle that drawn the air with high ambient temperature, as shown in Figure 20. Thus, the coolant water flows through the dehumidifier extracts sensible heat rather than latent heat, leading to more condensation of the water vapour. Besides, the figure shows that the DBT of air is almost constant throughout the day.

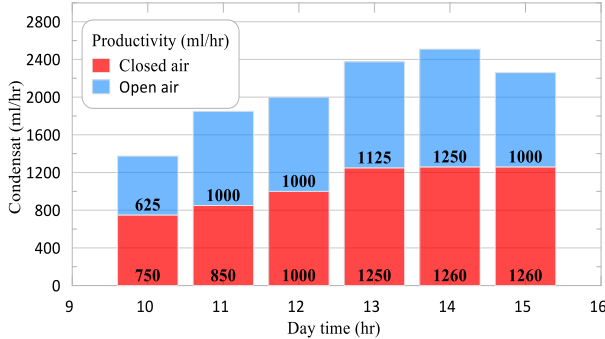
Figure 21 shows the air humidification and dehumidification processes through the desalination unit for 9, 13 and 15 hr. The figure shows that the increase in dry bulb temperature is the sensible heating, and the air's high moisture content represents latent heat. Removing most of the moisture content reflects an excellent performance to the dehumidifier; so, HDH processes' performance is the best at the time 13 hr. The improvement in the HDH at time 13 hr is due to the high salty water temperature at this time, as indicated in Figure 16.



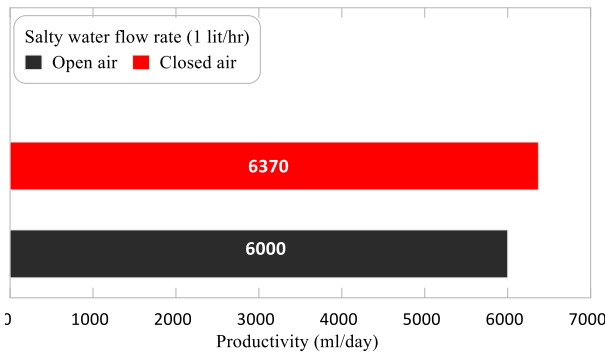
**Fig. 16** The effect of salty water temperature on the outlet air conditions from the humidifier



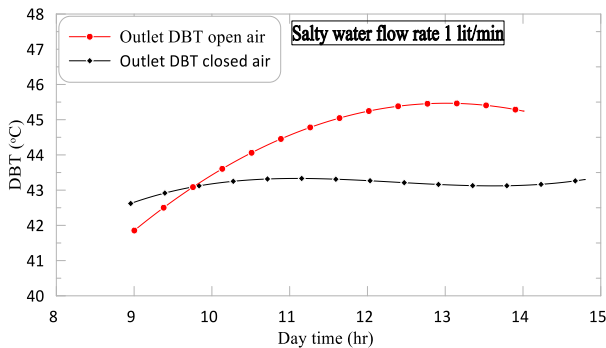
**Fig. 17** The variation of inlet and outlet water from the dehumidifier with time



**Fig. 18** Comparison between the hourly productivity of open and closed air cycle for the salty water flow rate of 1 lit/min



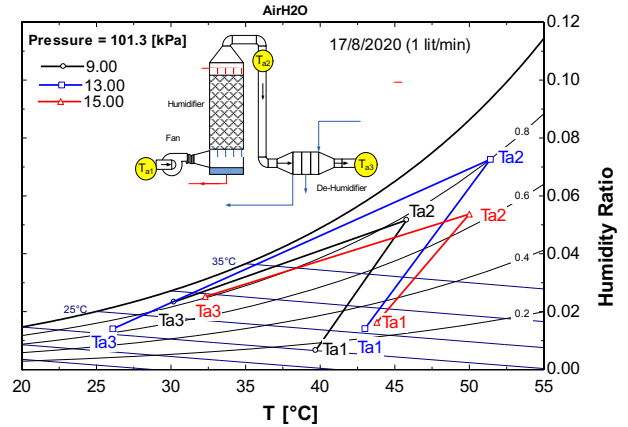
**Fig. 19** Comparison between the daily productivity of open and closed air cycle for the salty water flow rate of 1 lit/min



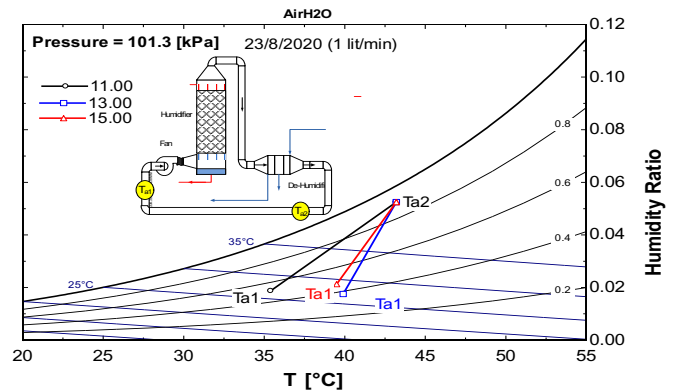
**Fig. 20** Comparison between the outlet DBT of leaving air from humidifier for open and closed air cycle for the salty water flow rate of 1 lit/min

Figure 22 shows the HDH process for the closed air cycle. It can be seen from the figure that the entering DBT of air is less than that of the ambient air. In contrast, the leaving air condition is almost constant regardless of inlet air conditions, which gave a dehumidifier's uniform performance.

Figure 23 shows a comparison between the current work and Juarez-Trujillo et al., 2011 (Juarez-Trujillo, Martin-Dominguez and Alarcón-Herrera, 2011), it can be seen from the figure that the trends of both HDH units are the same, but the productivity of Juarez-Trujillo et al is more than the productivity of the current work by about 14 to 20%, since the previous work uses the solar radiation to heat up a storage tank for the salty water.



**Fig. 21** The HDH processes for the desalination unit for three selected day time



**Fig. 22** The HDH processes through the HDH unit for a closed air cycle.

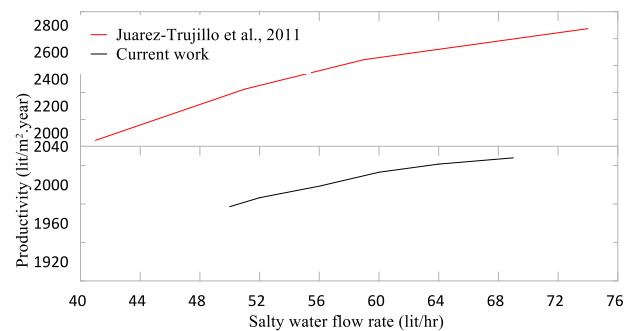


**Fig. 23** Comparison with other work

## 5. CONCLUSIONS

- From the work results, it can be concluded that
1. The best volume of salty water flows through the PTSC and humidifier is 1 lit/min. This can produce 6.37 lit/day (during the testing period 6 hour a day), with average daily water productivity of 1.062 lit/hr in August 2020.
  2. Increasing the salty water flow rate above 1 lit/min deteriorates the productivity of freshwater.

- The best configuration of the air-water cycles is the closed air open water (CAOW) circuit. This can produce about 6.37 lit/day of freshwater when the salty water flow rate is lit/min.
- Using the closed air circuit provides a uniform condition for the saturated air leaving the humidifier.

### ACKNOWLEDGEMENTS

We would like to express our thanks to the respected editors of International Journal Frontiers in Heat and Mass Transfer and the respected reviewers for their comments that clearly enhance the manuscript. Also, we would like to thank our institution Al-Mustaqbal University College" for the financial support ([www.mustaqbal-college.edu.iq](http://www.mustaqbal-college.edu.iq))

### NOMENCLATURE

$a$	Surface area per unit volume ( $m^{-1}$ )
$A_{abs}$	Area of the absorber ( $m^2$ )
$A_g$	Area of the glass cover ( $m^2$ )
$A_a$	Collector aperture area ( $m^2$ )
$c_{pa}$	Specific heats of air (kJ/kg.K)
$c_{pv}$	Specific heats water vapor (kJ/kg.K)
$c_{pf}$	Specific heat of the working fluid (kJ/kg.K)
$D_{abs,o}$	Outside diameter of the absorber (m)
$D_{abs,i}$	Inner diameter of the receiver (m)
$D_g$	Glass cover diameter (m)
$D_{g,in}$	Inside diameter of the glass cover (m)
$dL$	Increment in the mass flow rate of water (kg/s)
$R_{ab}$	Rayleigh number
$F'$	Collector efficiency factor
$F''$	Collector flow factor
$f_f$	Friction factor
$F_R$	Heat removal factor
$g$	Gravitational acceleration ( $m/s^2$ )
$G$	Mass flow rate of air through the humidifier (kg/s)
$h_{c,g-amb}$	Convection heat transfer coefficient between glass and ambient ( $W/m^2.K$ )
$h_{ci}$	Inner heat transfer coefficient of the dehumidifier tube ( $W/m^2.K$ )
$h_{co}$	Outer heat transfer coefficient of the dehumidifier tube ( $W/m^2.K$ )
$h_{diff}$	Mass transfer coefficient ( $kg/m^2s$ )
$h_f$	Heat transfer coefficient inside the tube ( $W/m^2.K$ )
$h_{r,g-amb}$	Radiation heat transfer coefficient between the glass and the ambient ( $W/m^2.K$ )
$I_b$	Beam solar radiation ( $W/m^2$ )
$k_{abs}$	Thermal conductivity of absorber ( $W/m.K$ )
$k_c$	Thermal conductivity of the copper tube ( $W/m.K$ )
$k_{ff}$	Effective thermal conductivity that the stationary air ( $W/m.K$ )
$k_a$	Thermal conductivity of air ( $W/m.K$ )
$L$	Mass flow rate of water through the humidifier (kg/s)
LMTD <sub>c</sub>	Logarithmic mean temperature difference between coolant water and air (K)
$m_{cw}$	Mass flow rate of coolant water (kg/s)
$Nu_a$	Nusselt number of air
$Pr_{air}$	Prandtl number of air in the annular
$Q_u$	Useful heat gain by the water (W)
$r_{ci}$	Inner radius of the heat exchanger tubes (m)
$r_{co}$	Outer radius of the heat exchanger tubes (m)
$Re_a$	Reynolds number of air
$Rf_c$	Fouling factor thermal resistance (m.K/W)
$T_{abs}$	Absorber temperature (K)
$T_{ac}$	Saturated air temperature (K)
$T_{amb}$	Ambient temperature (K)

$T_{cwi}$	Inlet coolant water temperature (K)
$T_{r,i}$	Inlet water temperatures (K)
$T_{r,o}$	Outlet water temperature (K)
$T_g$	Glass cover temperature (K)
$T_{cwo}$	Outlet coolant water temperature (K)
$U_o$	Outlet coolant water temperature ( $W/m^2 \cdot K$ )
$V$	Volume of packing ( $m^3$ )
$V_a$	Velocity (m/s)

### Greek Symbols

$\alpha_{air}$	Thermal diffusivity of air ( $m^2/s$ )
$\beta_{air}$	Volumetric thermal expansion coefficient of air ( $K^{-1}$ )
$d\omega$	Increment in the moisture content of the air (kgw/kg)
$\epsilon_{abs}$	Emissance of absorber
$\epsilon_g$	Emissance of the glass cover
$\mu_a$	Viscosity of air, respectively (Pa.s)
$\rho$	Density of air ( $kg/m^3$ )
$\sigma$	Stefan-Boltzmann constant ( $W/m^2 \cdot K^4$ )
$\nu_{air}$	Kinematic viscosity of air ( $m^2/s$ )

### REFERENCES

- Al-Enezi, G., Ettouney, H. and Fawzy, N. (2006) 'Low temperature humidification dehumidification desalination process', *Energy Conversion and Management*, 47(4), pp. 470–484. <https://doi.org/10.1016/j.enconman.2005.04.010>
- Duffie, J. A. and Beckman, W. A. (2013) *Solar Engineering of Thermal Systems*. John Wiley & Sons.
- El-Agouz, S. A. (2010) 'A new process of desalination by air passing through seawater based on humidification-dehumidification process', *Energy*, 35(12), pp. 5108–5114. <https://doi.org/10.1016/j.energy.2010.08.005>
- Ettouney, H. (2005) 'Design and analysis of humidification dehumidification desalination process', *Desalination*, 183(1–3), pp. 341–352. <https://doi.org/10.1016/j.desal.2005.03.039>
- Garg, H. (2000) *Solar energy: fundamentals and applications*. Tata McGraw-Hill Education.
- Garg, H. P. and Prakash, J. (1997) *Solar energy: fundamentals and applications*. Tata McGraw-Hill.
- He, W. F. et al. (2017) 'Performance analysis of a solar-driven humidification dehumidification desalination system in summertime', in *2017 IEEE International Conference on Smart Grid and Smart Cities, ICSGSC 2017*. Institute of Electrical and Electronics Engineers Inc., pp. 33–36. <https://doi.org/10.1109/ICSGSC.2017.8038545>.
- Jacobson, E. et al. (2006) 'Solar parabolic trough simulation and application for a hybrid power plant in Thailand', *ScienceAsia*, 32, pp. 187–199. <https://doi.org/10.2306/scienceasia1513-1874.2006.32.187>.
- Juarez-Trujillo, A., Martin-Dominguez, I. R. and Alarcón-Herrera, M. T. (2011) 'Using TRNSYS Simulation to Optimize the Design of a Solar Water Distillation System', in *ISES Solar World Congress*. Kassel, Germany: ISES.
- Kabeel, A. E. and El-Said, E. M. S. (2013) 'A hybrid solar desalination system of air humidification–dehumidification and water flashing evaporation', *Desalination*, 320, pp. 56–72. <https://doi.org/10.1016/j.desal.2013.04.016>.
- Kalogirou, S. A. et al. (2016) 'Exergy analysis of solar thermal collectors and processes', *Progress in Energy and Combustion Science*. Elsevier Ltd, pp. 106–137. <https://doi.org/10.1016/j.peccs.2016.05.002>.
- Kreith, F., Manglik, R. and Bohn, M. (2012) *Principles of heat transfer*. 8th edn. Cengage Learning.

- Li, M. and Wang, L. L. (2006) 'Investigation of evacuated tube heated by solar trough concentrating system', *Energy Conversion and Management*, 47(20), pp. 3591–3601. <https://doi.org/10.1016/j.enconman.2006.03.003>.
- Mahmoud, A., Fath, H. and Ahmed, M. (2018) 'Enhancing the performance of a solar driven hybrid solar still/humidification-dehumidification desalination system integrated with solar concentrator and photovoltaic panels', *Desalination*, 430, pp. 165–179. <https://doi.org/10.1016/j.desal.2017.12.052>.
- Manjunath, M. S. *et al.* (2020) 'Experimental study of the influence of glass cover cooling using evaporative cooling process on the thermal performance of single basin solar still', *Journal of Mechanical Engineering and Sciences*, 14(1), pp. 6334–6343. <https://doi.org/10.15282/jmes.14.1.2020.11.0496>.
- Mayer, A. (2011) *Solar powered desalination*. University of Nottingham.
- Mazloumi, M., Naghashzadegan, M. and Javaherdeh, K. (2008) 'Simulation of solar lithium bromide-water absorption cooling system with parabolic trough collector', *Energy Conversion and Management*, 49(10), pp. 2820–2832. <https://doi.org/10.1016/j.enconman.2008.03.014>.
- Moumouh, J., Tahiri, M. and Balli, L. (2018) 'Solar Desalination by Humidification-Dehumidification of Air', *MATEC Web of Conferences*. Edited by A. Diouri *et al.*, 149, p. 02092. <https://doi.org/10.1051/mateconf/201814902092>.
- Narayan, G. P. *et al.* (2010) 'The potential of solar-driven humidification-dehumidification desalination for small-scale decentralized water production', *Renewable and Sustainable Energy Reviews*, pp. 1187–1201. <https://doi.org/10.1016/j.rser.2009.11.014>.
- Nawayseh, N. K. *et al.* (1999) 'Solar desalination based on humidification process - I. Evaluating the heat and mass transfer coefficients', *Energy Conversion and Management*, 40(13), pp. 1423–1439. [https://doi.org/10.1016/S0196-8904\(99\)00018-7](https://doi.org/10.1016/S0196-8904(99)00018-7).
- Orfi, J., Galanis, N. and Laplante, M. (2007) 'Air humidification-dehumidification for a water desalination system using solar energy', *Desalination*, 203(1–3), pp. 471–481. <https://doi.org/10.1016/j.desal.2006.04.022>.
- Orfi, J., Laplante, M. and Marmouch, H. (2004) 'Experimental and theoretical study of a humidification-dehumidification water desalination system using solar energy', *Desalination*, 168(1–3), pp. 151–159. <https://doi.org/10.1016/j.desal.2004.06.181>.
- Pourafshar, S. T., Jafarinaemi, K. and Mortezaipoor, H. (2020) 'Development of a photovoltaic-thermal solar humidifier for the humidification-dehumidification desalination system coupled with heat pump', *Solar Energy*, 205, pp. 51–61. <https://doi.org/10.1016/j.solener.2020.05.045>.
- Sachdev, T., Gaba, V. K. and Tiwari, A. K. (2020) 'Performance analysis of desalination system working on humidification-dehumidification coupled with solar assisted air heater and wind tower: Closed and open water cycle', *Solar Energy*, 205, pp. 254–262. <https://doi.org/10.1016/j.solener.2020.04.083>.
- Shalaby, S. M., Bek, M. A. and Kabeel, A. E. (2017) 'Design Recommendations for Humidification-dehumidification Solar Water Desalination Systems', in *Energy Procedia*. Elsevier Ltd, pp. 270–274. <https://doi.org/10.1016/j.egypro.2016.12.148>.
- Stoecker, W. and Jones, J. (1982) *Refrigeration and air conditioning*. 2nd edn. McGraw-Hill.
- Thepa, S. *et al.* (1999) 'Improving indoor conditions of a Thai-style mushroom house by means of an evaporative cooler and continuous ventilation', *Renewable Energy*, 17(3), pp. 359–369. [https://doi.org/10.1016/S0960-1481\(98\)00761-7](https://doi.org/10.1016/S0960-1481(98)00761-7).
- Yamali, C. and Solmuş, I. (2007) 'Theoretical investigation of a humidification-dehumidification desalination system configured by a double-pass flat plate solar air heater', *Desalination*, 205(1–3), pp. 163–177. <https://doi.org/10.1016/j.desal.2006.02.053>.
- Yuan, G. *et al.* (2011) 'Experimental study of a solar desalination system based on humidification-dehumidification process', *Desalination*, 277(1–3), pp. 92–98. <https://doi.org/10.1016/j.desal.2011.04.002>.